Visualisation and performance evaluation of biodiesel/methane co-combustion in a swirl-stabilised gas turbine combustor

Ogbonnaya Agwu[a,b,*], Jon Runyon[a], Burak Goktepe[a], Cheng Tung Chong[c], Jo-Han Ng[d], Anthony Giles[a], Agustin Valera-Medina[a]

[a]*School of Engineering, Cardiff University, Wales, UK*
[b]*Department of Mechanical Engineering, University of Uyo, Uyo, Nigeria*
[c]*China-UK Low Carbon College, Shanghai Jiao Tong University, Lingang, Shanghai, China*
[d]*Faculty of Engineering and Physical Sciences, University of Southampton Malaysia, Malaysia*
*Corresponding author. Email: AgwuOE@cardiff.ac.uk

Abstract

While dual fuel firing of power generation combustion systems can provide energy security by improving the fuel flexibility of such systems, several studies on compression ignition engines have also shown a positive impact on NO_X and PM emissions. Previous multiphase fuel combustion studies for gas turbine engines are limited, thus the present study addresses that gap by fuelling a model swirl stabilised gas turbine combustor with a blend of waste cooking oil-derived biodiesel and methane. Increasing amounts of methane were injected into the swirling combustion air flow while simultaneously reducing the biodiesel spray flowrate across a pressure atomiser, thus maintaining an overall thermal power output of 15 kW and a global equivalence ratio of 0.7 in all cases, except for flame stability range trials. Direct flame imaging, C_2* and CH* chemiluminescence imaging, post combustion emissions as well as stability performance of the flames were evaluated. Emissions results indicate a reduction in NO_x emissions whereas unburned hydrocarbons emissions increased when the dual fuel tests were compared with neat biodiesel combustion with further reduction of these emissions as gas fraction in the fuel mix increases. Further, flame images suggest increased wrinkling and perturbing of the flame front as gas fraction of the biodiesel/methane flame increases. However, the temporal variation of integral intensity of C_2* and CH* species chemiluminescence point to lesser fluctuation in the rate of heat release hence improved flame stability and reduced combustion noise as methane partially replaces biodiesel in the combustion process. Also, it was found that flame stability limits reduce as methane partly replaces biodiesel in the flame; an average of 17% decrement in lean extinction limit is observed as methane content of combusted fuel increases from 0 to 20%.

Keywords: alternative fuel, combustion, emissions, multiphase, stability

1 Introduction

Across the globe, the search for greener means of energy generation, driven by the ever-growing call for environmental sustainability, has led down several pathways. One such pathway has been the exploration of sustainable biodiesel for use in combustion systems. For instance, based on comparable engine performance obtained, Chauhan et al. [1] opined that biodiesel refined from non-edible jatropha oil has good potential of substituting for diesel in compression ignition engines without any engine modification. Also, Hashimoto et al. [2] found that the combustion of palm methyl esters under gas turbine conditions is similar in several ways to that of fossil diesel and therefore a 'promising alternative fuel for gas turbines' [2]. Further, extensive research has been conducted into the emissions performance of

biodiesel compared to fossil diesel. Several studies [3-8] reached the conclusion that carbon monoxide (CO), unburned hydrocarbon (UHC) and particulate matter (PM) emissions reduced whereas NO_x emissions increased when replacing diesel with biodiesel in compression ignition (CI) engines. Moreover, in experiments comparing diesel with biodiesel conducted in replications of gas turbine combustors, biodiesel combustion resulted in lower NO_x and CO emissions [2,9,10]. However, not all published works are in agreement with the highlighted trend of emissions when biodiesel combustion is compared with that of diesel in internal combustion engines. For example, Chong and Hochgreb [11], who investigated combustion characteristics of rapeseed methyl esters in model gas turbine combustors, reported lower NO_x emissions when compared with diesel burn; they also reported higher CO emissions – opposite to most studies. This is not peculiar to Chong and Hochgreb [11], and it is possible that different trends might be observed because different studies employ unique operational strategies and materials [12,13].

Another argument often employed in advocating for increased use of biofuels is its touted lower greenhouse gas (GHG) emissions [14,15]. Studies show that 3 kg of CO_2 is emitted per litre of biodiesel combusted, 5% less than the corresponding emission from the same volume of fossil diesel [16], but that is without taking account of factors like biodiesel feedstock carbon sequestration during growth (assuming plant feedstock), impact of land use change and fuel production operations. Clearly, without a comprehensive life cycle analysis on a case by case basis for the different varieties of biodiesel, there is scope for debate regarding the carbon footprint of diesel versus biodiesel. Useful as such an analysis might be, it would seem that the most efficient way of reducing GHG emissions from the combustion of carbon rich fuels like diesel or biodiesel is by simply decreasing the amount of it consumed. A seemingly strong argument would be to depend entirely on low carbon fuels like natural gas (NG) or indeed carbon neutral fuels, however a single fuel cannot meet the ever increasing energy demand, particularly across sectors. This interplay of factors has led to investigations into dual fuel, multiphase combustion in engines that hitherto operate on a single fuel.

There are several studies in multiphase fuel combustion in CI engines [17-20], and a common operating technique is to utilise diesel in small amounts as the ignition source while injecting NG into the intake passage to form a premixed fuel-air charge. Diesel/natural gas co-combustion experiments in diesel engines generally result in significantly lower CO_2, NO_x and PM emissions yet higher HC and CO emissions in comparison with regular diesel combustion [21]. Dual fuel experiments in gas turbine combustor conditions are often single phase blends of two different fuels [22-25]. However, in view of rising energy demands and the need to guarantee energy security, there will be increasing demand for gas turbines to demonstrate improved fuel flexibility in the context of dual phase fuel burn. In this regard though, published research is limited. Sidey and Mastorakos [26] studied ethanol-methane-air flames and detailed flame structure and stability variation with changes in methane fraction. Similarly, *n*-heptane-methane flames were examined, noting stabilisation issues and flame structure differences as a result of dual phase fuel combustion [27]. Further, Evans et al. [28] detailed the impact of adding hydrogen to the dual-fuel flame of Sidey and Mastorakos [27] by imaging temperature and reaction zone conditions of the resultant flame.

The present study aims to address the identified gap in the literature by means of systematic, parametric investigation. In the first instance, the study aims to quantify how both flame structure and reaction zone change in a biodiesel spray flame burning in a swirling premixed methane-air coflow by means of both direct flame imaging and CH^*/C_2^* chemiluminescence imaging. Furthermore, this study evaluates the impact of dual fuel co-combustion on

regulated emissions including NO_x and UHCs. Increasing amounts of methane were added to the swirling oxidiser stream while decreasing the flow rate of biodiesel across the spray nozzle so that, for all emissions test cases, an overall heat output of 15 kW is maintained at a global equivalence ratio, φ_{global}, of 0.7. Exploring multiphase fuelling of gas turbines by testing practical fuels like biodiesel and methane is important not just for the potential of expanding the fuel flexibility of such systems, but also data acquired from studies like the present one can help validate turbulent multiphase fuel combustion numerical modelling, when considered alongside flow field and spray characterization experiments.

2 Method

2.1 Burner Description

A model swirl-stabilised gas turbine combustor (Fig. 1) was used in this study in which biodiesel spray was combusted in premixed air/methane flow. The biodiesel spray was achieved using a Delavan 0.4 GPH 60° W nozzle; the liquid flow rate across the nozzle being controlled by means of a Bronkhorst mini CORI-FLOW M1x mass flow controller (MFC) with a rated accuracy of ±0.2% of indicated reading. The liquid fuel supply to the MFC, in turn, was via an upstream Walbro GSL392 inline fuel pump with the fuel delivery pressure to the MFC set at 0.85 MPa.

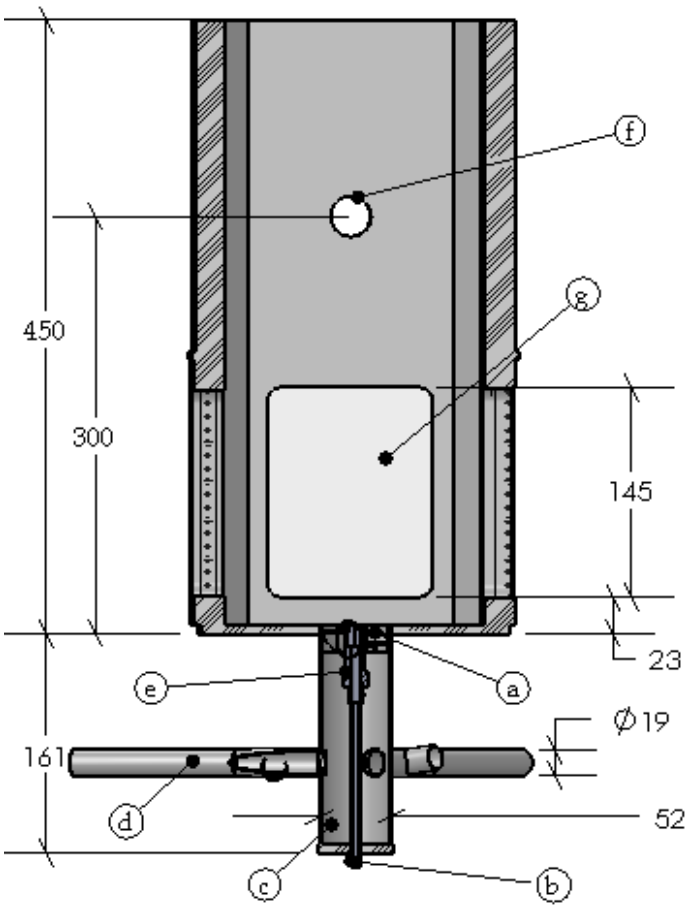

Fig. 1. Dual phase burner 2D section view. (a) axial swirler (b) liquid fuel line (c) inlet plenum (d) combustion air/methane inlet (e) pressure atomiser (f) emissions probe slot (g) quartz window. All dimensions in millimetres.

Methane and air were mixed in the burner plenum having been supplied to the system at room temperature and metered by variable area rotameters in the range 1-12 l/min for methane and 30-150 l/min as well as 40-440 l/min for air with accuracies of ±1.25% FSD for the lower flow range and ±5% FSD for the higher flow range. The gases are further mixed as they pass through an axial swirler that sits flush with the nozzle orifice plane. The swirler has a tip diameter, D_s, of 50 mm and a hub diameter, D_h, of 16 mm. It has five swirl vanes each about 2 mm thick. The angle of swirl, θ, is 60° so that from Eq. (1), the geometric swirl number (S_N) is 1.24.

$$S_N = \frac{2}{3}\left[\frac{1-(D_h/D_s)^3}{1-(D_h/D_s)^2}\right]\tan\theta \qquad (1)$$

The chamber where combustion occurs has a square cross-section of sides 180 x 180 mm and height of 450 mm with a 100 x 145 mm quartz window on each of its four sides. The base of each quartz window is 23 mm from the dump plane of the combustor, thus no optical access is possible below that point.

2.2 Fuels

Table 1 provides the relevant properties of the tested fuels – biodiesel and methane. The biodiesel was obtained from Olleco (UK) who state it is methyl esters from lipid sources produced as per EN 14214 standard. Derived from waste cooking oil, the biodiesel can be classified as second generation type according to Atabani et al. [29]. Utilised methane was of CP grade and obtained from BOC Limited.

Table 1. Fuel properties [11,30]

Property	Biodiesel	Methane
Approximate chemical formula	$C_{19}H_{36}O_2$	CH_4
Lower Heating Value, LHV (KJ/kg)	36800	50000
Density at 15°C (kg/m^3)	880	0.656
Stoichiometric fuel-air ratio (mass basis)	0.080	0.058
Kinematic Viscosity, υ (mm^2/s)	6.75	17.08
Surface Tension, σ (kg/s^2)	0.032	0.014
Flash Point (^{0}C)	145	-188

Apart from the flame stability range experiments, the premixed swirling methane-airflow together with the biodiesel spray were selected to deliver an overall power output of 15 kW at a φ_{global} = 0.7. The ratio of liquid to gaseous fuel for the constant power output cases was varied from 100/0 to 70/30 in steps of 10%. The fuel combinations were based on heat output share ratio. For instance, a 90/10 combination means that 90% of the overall heat output is set to be supplied by the biodiesel and the balance obtained from the methane. The total heat output of both fuels in each case was maintained at 15 kW and the calculation was based on the LHV of the fuels according to Eq. (2) in which $\dot{m}$ represents the mass flow rate of fuel and the subscripts l and g represent liquid and gas, respectively.

$$THO = (LHV_l \times \dot{m}_l) + (LHV_g \times \dot{m}_g) \qquad (2)$$

Table 2 provides details of fuel combination for the different biodiesel/methane flame experimental cases.

Table 2. Flame fuel combinations for 15 kW and φ_{global} = 0.7

Liquid/gas fuel proportion	Flow rates			Pressure drop across nozzle, ΔP (kPa)
	Biodiesel (g/s)	Methane (l/min)	Air (l/min)	
100/0	0.41	0.0	357	850
90/10	0.37	2.7	357	750
80/20	0.33	5.5	358	600
70/30	0.29	8.2	358	380

The relevant air flow rate based on φ_{global} in the combustion chamber was calculated according to Eq. (3).

$$\dot{m}_{air} = \frac{\dot{m}_g \times AFR_{Stoic,g} + \dot{m}_l \times AFR_{Stoic,l}}{\varphi_{global}} \quad (3)$$

$$SMD = 7.3{\sigma_l}^{0.6}{\nu_l}^{0.2}{\dot{m}_l}^{0.25}\Delta P^{-0.4} \quad (4)$$

Radcliffe's SMD correlation equation (Eq. 4), proven in [31] to best predict Sauter mean diameter (SMD) of spray droplets for the type of nozzle utilised in the present study, was used to estimate the variation of SMD as liquid flow rates change based on the fuel combinations tested.

2.3 Flame Luminescence and Emissions Measurements

For flame chemiluminescence measurements, a LaVision Imager Intense CCD camera coupled with a LaVision IRO Intensifier was used with a 60 mm focal length AF Micro-Nikkor (f/2.8) lens. The camera was focused at the centreline of the burner capturing a plane that is ±50 mm in the radial direction and 140 mm in the axial direction from the base of burner optical window; the setup resulted in a resolution of 0.12 mm/pixel. C_2* and CH* chemiluminescence emissions were acquired by separately fitting bandpass filters of 515 nm (FWHM = 10 nm) and 430 nm (FWHM = 10 nm), respectively, on the lens. The species C_2* and CH* were selected because both have been identified to be good indicators of heat release rate in hydrocarbon flames [11,32,33]. The emissions spectra of C_2* radicals are not only more prominent than that of OH* in liquid fuelled combustors [34], but also they are spectrally resolved with a clearly identifiable peak at 516 nm. CH* radicals, at 431 nm on the other hand, have been used to explore the combustion of gaseous hydrocarbon flames [33,35]. The intensifier gate time was set at 80 μs and gain held constant across all experimental conditions based on optimisation studies previously carried out. For each experimental condition, 250 images were captured at 10 Hz. The images were then time averaged, background corrected and cropped using LaVision DaVis 7 software. The resulting chemiluminescence images were then Abel transformed using the MATLAB code developed by Runyon et al. [36] assuming flames were axisymmetric about the burner centreline. Broadband flame luminosity images were captured using an Olympus OM-D E-M5 Mark II camera with a M.Zuiko Digital 45 mm f/1.8 lens with an exposure time of 1/8000 s.

Post combustion emissions (NO_x and UHCs) were measured 300 mm from the nozzle orifice plane using a Testo 350 XL emissions analyser. The control unit of the device was programmed to sample flue gas for a duration of two minutes for each test condition at measuring rate of 3 seconds. It was noted that of the 40 readings taken at each experimental condition, the data stabilized well before the last 20 readings, and as such the average of the

last 20 readings are reported. Further, the emissions analyser was set to an oxygen reference of 15%. Equipment calibration estimated a ±5% measurement uncertainty for the presented emissions.

2.4. Chemical Kinetics Analysis

Chemical kinetics modelling was conducted to determine the trend of volumetric heat release and adiabatic flame temperature for the biodiesel and biodiesel/methane flames experimentally studied. CHEMKIN-PRO suite [37] was utilised for the numerical study with fuel combinations and operating conditions set as in the experiments with the solution based on an adaptive grid of 1000 points. The biodiesel mechanism used was developed by the CRECK modelling group [38] and comprises of 177 species and 2904 reactions. Although biodiesel combustion kinetics involve several hundred to thousands of species, the reduced mechanism of Ranzi et al. [38] was achieves reasonable simulation accuracy of main combustion properties [39] and has been referenced in works like [40] and [41].

3 Results and Discussion

3.1 Flame Stability Limits

The method used in delineating the region of stable burning in the combustion experiments was adapted from that outlined in Lefebvre and Ballal [42]. In the present stability study, flames at heat outputs of 6, 8, 10, 12, 14 and 16 kW were established, and for each heat output, the air flow rate was gradually increased lean until flame extinction occurred. Also, after re-establishing the flame at the same heat output, the air flow rate was gradually reduced up to the rich extinction point which was noted as well. This process was repeated for the aforementioned levels of power output for the 100/0 and 90/10 cases. The 6 kW test was omitted for the 80/20 case as a stable flame could not be sustained at the corresponding fuel flow rates possibly due to deterioration of spray quality with reduction in biodiesel flowrate. Similarly, combustion of the 70/30 case proved to be highly inefficient at the lower range of heat output up to 12 kW. The fuel lean and fuel rich extinction points result in the curves of Fig. 2 for three different fuel combinations. It can be observed in Fig. 2 that there is a reduction in the region of stable burning – the area under each curve – as methane replaces biodiesel as a fraction of the thermal power output. Further, as the fraction of methane increases in the combination, the flame stability limit (in terms of overall AFR) becomes narrower, particularly in the lean region. There is, on average, a 17% reduction in lean extinction limit as fuel composition changes from 100/0 to 80/20. The degradation in flame stability as combustion shifts from a single (liquid) fuel to dual fuel may be attributed to the alteration in flow dynamics as the swirling gaseous flow rate is increased [43,44]. The further contraction of stability range as gas percentage in fuel mix increases from 10% to 20% is attributable to, in addition to the foregoing, the loss in atomisation quality as liquid flow rate decreases. Decreasing the liquid flow rate causes a reduction in pressure drop across the nozzle as highlighted in Table 2. The resulting trend of SMD values as LGR changes shown in Fig. 3 means that liquid fuel evaporation rate is reduced as is the combustion rate which in turn leads to a decrease in the amount of recycled heat and chemical species necessary for anchoring and stabilising the flame. Further, the flame stability range contraction noted as gas flow rate increases is in agreement with the work of Valera-Medina et al. [44] who found that

swirl-stabilised reacting flows have increasingly weaker central recirculation zones as the local swirling fuel/air ratio increases.

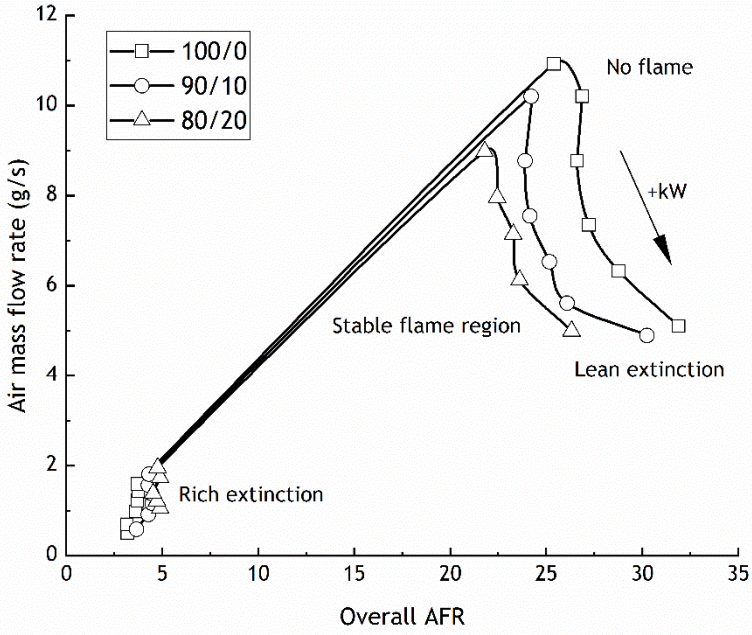

Fig. 2. Flame stability range as a function of overall AFR for biodiesel/methane flames of varying thermal power

The contraction of flame stability limits – and the associated issues – must be an important consideration for practical multiphase fuel combustors following the injection strategy utilised in this study and suggests that an alternative injection strategy might yield improved results.

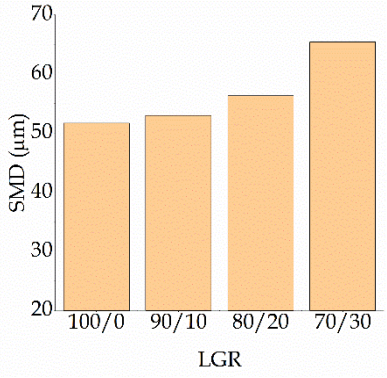

Fig. 3. SMD variation with combusted fuel liquid-to-gas ratio

3.2 Optical Emissions

The color flame luminosity images are combined with the corresponding C_2* and CH* chemiluminescence images in Fig. 4 for biodiesel/methane flames established at an overall heat output of 15 kW and φ_{global}= 0.7. The chemiluminescence images have been normalised to the maximum intensity in each species category. Both chemiluminescence species images show a reduction in intensity and area as gas content of fuel mix increases when considering the dual phase cases. The actual flame images appear to show first a wrinkling and then a seemingly turbulent separation of reacting flow that appears to worsen as fuel composition is altered from 100/0 to 90/10 and beyond.

A quantitative description of the variation in reaction zone properties is shown in Fig. 5. This includes each species integral intensity, defined in the same manner as Runyon et al. [36] as the pixel wise summation of each species intensity values from the temporally averaged and background corrected chemiluminescence images. An estimation of the reaction zone area and length was obtained from Fig. 6 which shows binary images of the corresponding Abel transformed chemiluminescence images. The binary images were generated in MATLAB by a global thresholding method. The Otsu thresholding method, which selects a threshold value that minimises the intraclass variance of the black and white pixels, was used holding the determined threshold constant across all images. The threshold value was based on the 100/0 image. The sum of the unity pixels in the images is designated as the reaction zone area whereas the distance between the uppermost unity pixel to the lowermost is regarded as the reaction zone length in each case.

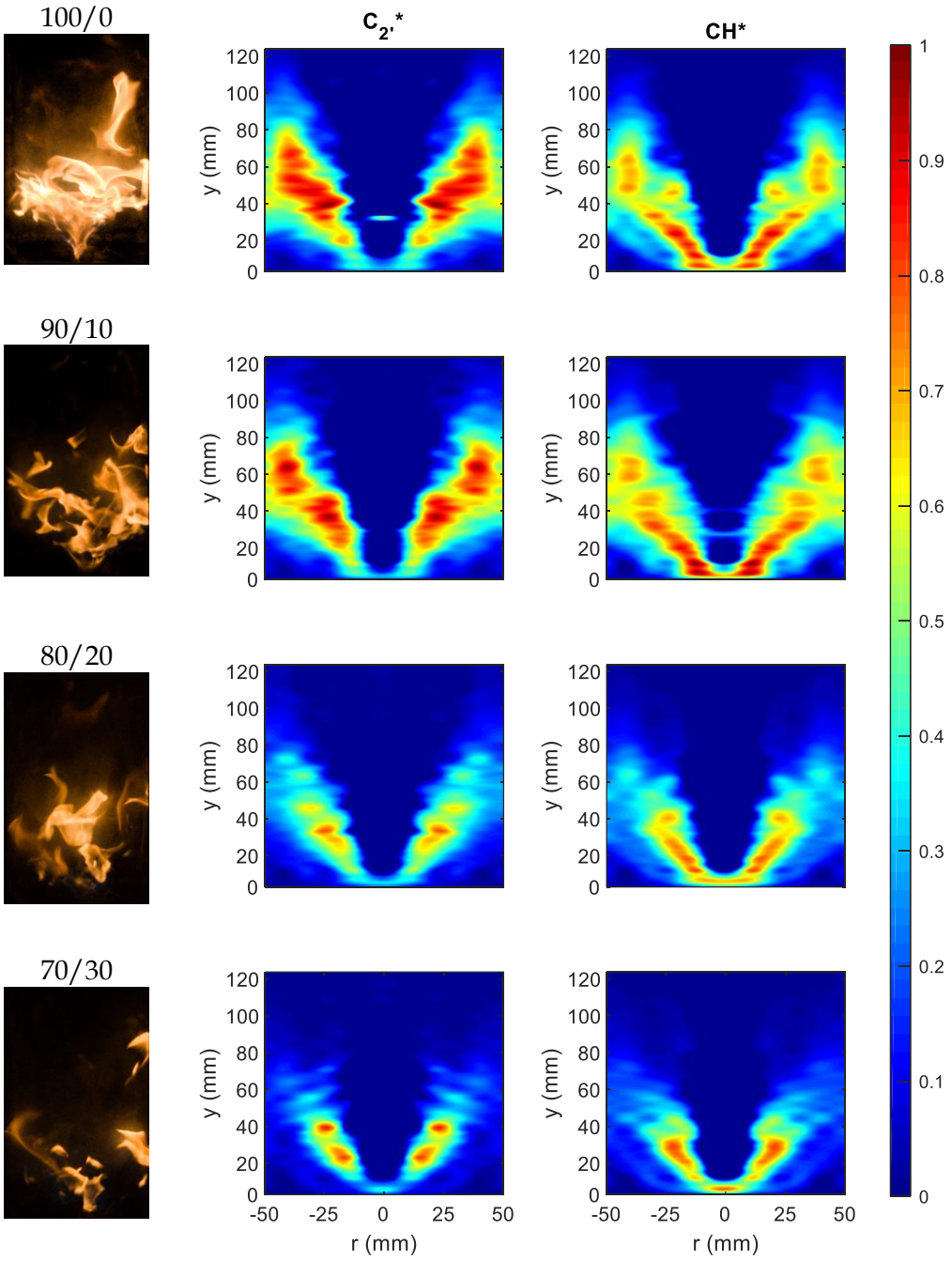

Fig. 4. Left column: Color flame images. Normalised Abel deconvoluted chemiluminescence images of C_2* (middle column) and CH* species (right column) in 15 kW biodiesel/methane flames at φ_{global} = 0.7. Flow is from bottom to top.

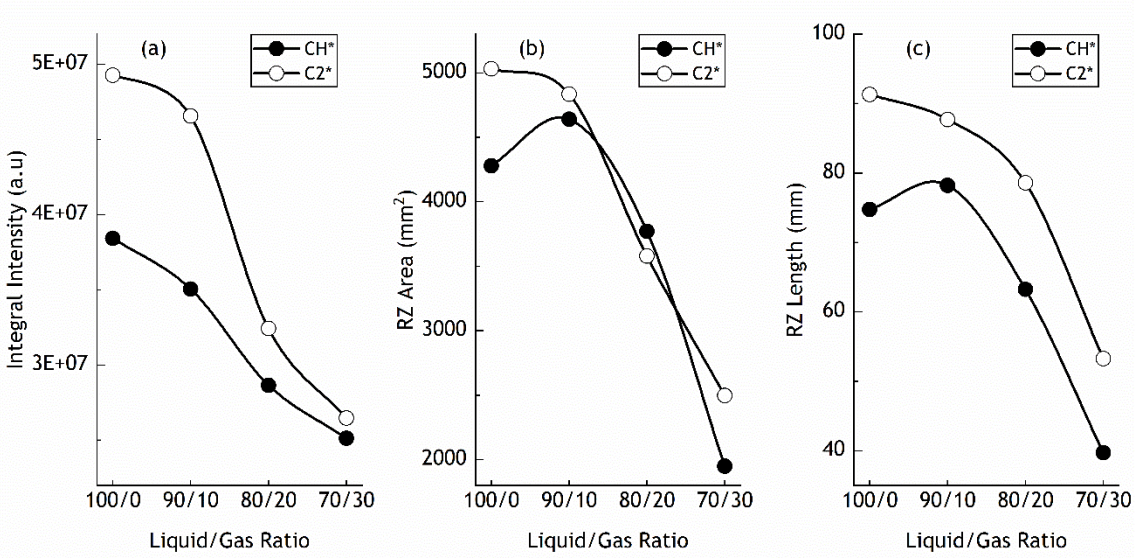

Fig. 5. Reaction zone properties: (a) species integral intensity, (b) reaction zone (RZ) area and (c) reaction zone length of 15 kW biodiesel/methane flames at $\varphi_{global} = 0.7$

The graphs of Fig. 5 suggest that the 90/10 biodiesel/methane combustion is not significantly different from neat biodiesel combustion. This suggests that, apart from the highlighted reduction in stable operational range, multiphase fuel burn in gas turbine combustors is possible without notable disturbance of the reaction zone at low gas fractions.
However, there is a sharp reduction in reaction zone area and length as liquid-gas ratio further decreases beyond 90/10. This considerable decline in reaction zone area and length may well be markers of overall decreased reactivity and flame residence time in the combustion process as C_2* and CH* are reasonably good indicators of the reaction zone of hydrocarbon flames.

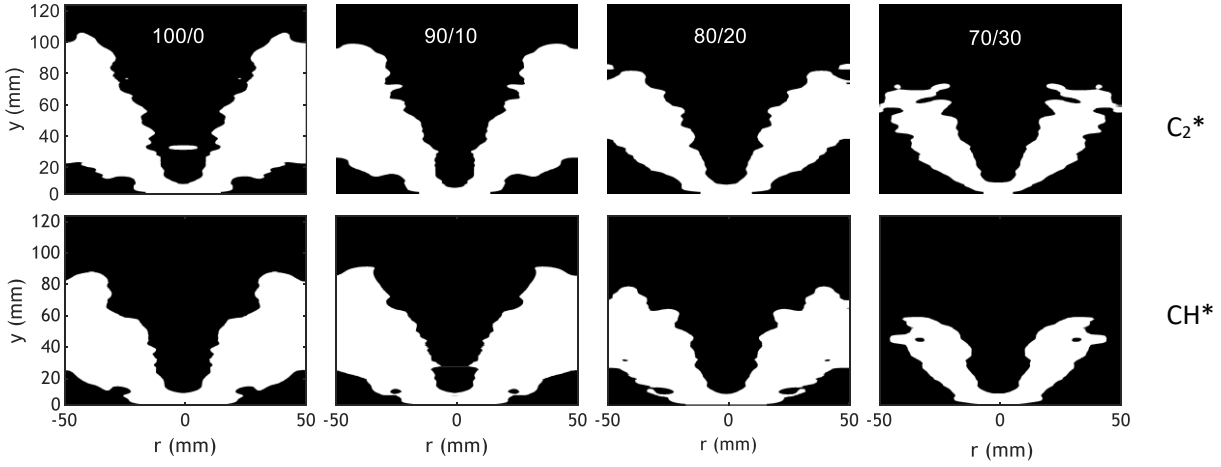

Fig. 6. Binary images of C_2* (top row) and CH* (bottom row) chemiluminescence in biodiesel/methane flames at different liquid/gas ratios. Flow is from bottom to top.

The temporal variation of the integral intensity of the chemiluminescence radicals can be assumed, similar to the approach in Ballester et al. [45], to be indicative of the variation of heat release rate from the flames. On this basis, the C_2* and CH* species integral intensity variation across the duration of the chemiluminescence imaging for each of the tested fuel combinations was calculated and compared. Samples of this fluctuation in the rate of heat release is shown in Fig. 7; the C_2* integral intensity variation over time is shown for the 100/0 case in Fig. 7(a) and for the 70/30 case in Fig. 7(b). The corresponding data for the CH* species is shown in Fig. 7(c) and 7(d) respectively. The solid horizontal line in each figure indicates the integral intensity of the average of the 250 images. As the average varies widely across the test cases, comparison of the data variability based on standard deviation is inadequate.

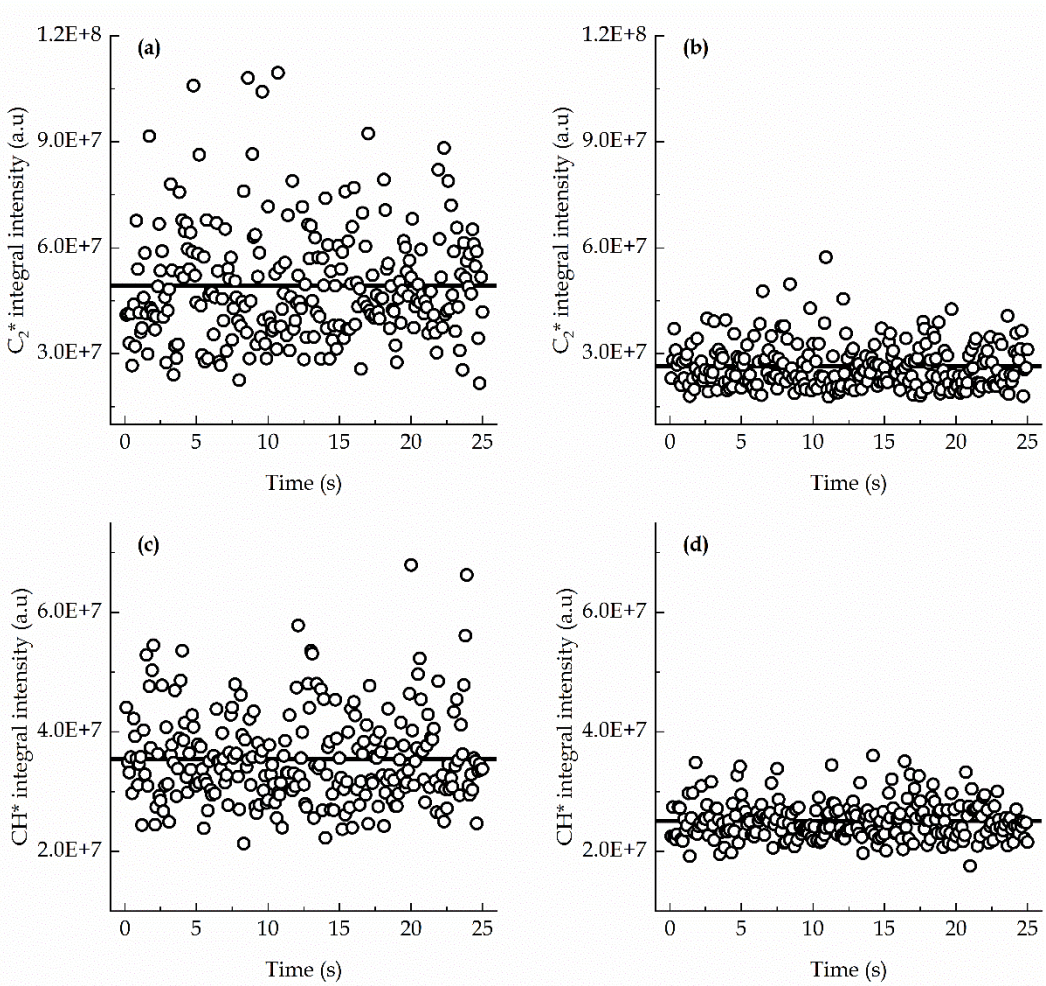

Fig. 7. Temporal fluctuation of chemiluminescence integral intensity for C_2* species (a) 100/0 and (b) 70/30 and CH* species (c) 100/0 and (d) 70/30 biodiesel/methane flames

Therefore the coefficient of variation (standard deviation normalised by mean value) has been employed. This is shown in Fig. 8 and points to lesser fluctuation in heat release rate as the percentage of methane in the multiphase fuel combustion increases. Decreased fluctuation in the rate of heat release improves flame stability and lessens combustion noise. The greater flame stability noted here as being occasioned by multiphase combustion must not be confused with the range of flame stability which was, in section 3.1, observed to contract as gas ratio in fuel mix increases.

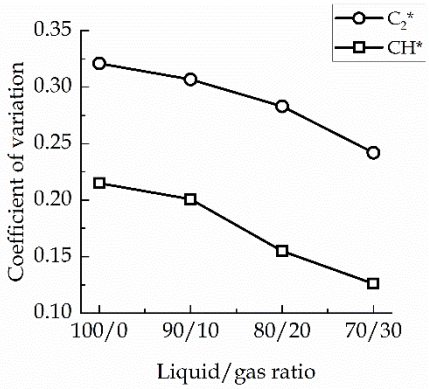

Fig. 8. Variability of species chemiluminescence integral intensity as a function of liquid/gas fuel ratio

3.3 Post Combustion Emissions

The apparent reduction in heat release rate and flame residence time is further supported by the post combustion emissions trend seen in Fig. 9: lower NO_x and higher UHC emissions as gas ratio increases. NO_x emissions are known to be heavily reliant on flame temperatures [46], for which heat release rate is important, and residence time. These two factors, on the basis of the optical emissions observed, appear to be reducing as the gaseous fuel component of the blend supplied for combustion increases. The assertion of lower flame temperatures and decreased heat release rate is supported by the chemical kinetics analysis shown in Fig. 10. Being a 1-D approach, the chemical kinetics simulation results in Fig. 10 must not be considered absolutes instead there are presented to show trends in the parameters considered.

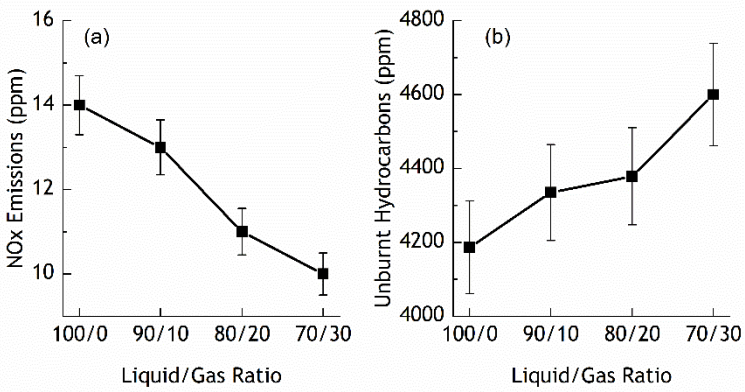

Fig. 9. Post combustion (a) NO_X and (b) UHC emissions in 15 kW biodiesel/methane flames at different liquid/gas ratios and $\varphi_{global} = 0.7$

As for UHCs, it would seem that the variation in flow dynamics particularly in the recirculation zone resulting from overall higher swirling flows as gas ratio increases [43,44] serve to discourage combustion particularly of the locally ultra-lean gas fuel sweeping it away from the combustion zone before it has any chance of burning. Moreover, as liquid flow rates drop with increasing gas ratio, the Sauter mean diameter of biodiesel droplets generated by the atomiser, shown in Fig. 3 to increase, leads to longer timescales for evaporation and subsequent combustion. The chemiluminescence and binary images showed that at higher gas ratios, there appears to be a diminishing of the reaction zone so that the longer time

required for the relatively larger droplets to vaporise and undergo combustion is unavailable. As a consequence, the unburned hydrocarbons emissions increase.

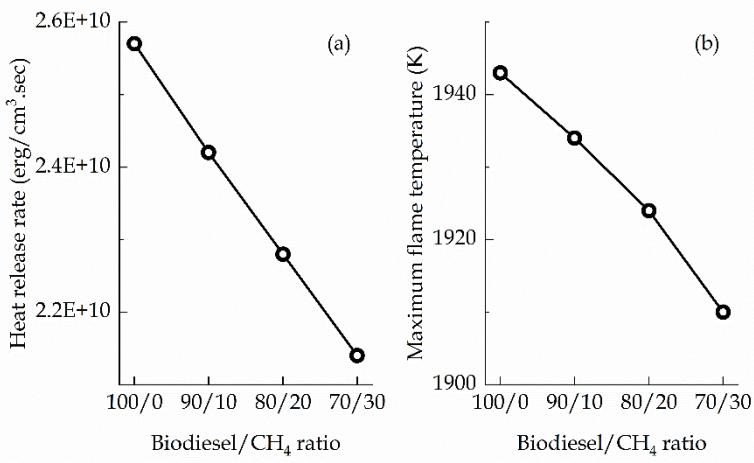

Fig. 10. Biodiesel/methane (a) volumetric heat release rate and (b) maximum flame temperature from chemical kinetics analysis.

Conclusions

Dual fuel multiphase combustion in a model gas turbine swirl-stabilised burner was carried out using biodiesel derived from waste cooking oil and methane, with the aim of partly replacing biodiesel with low C/H ratio methane in a bid to reduce carbon emissions and potentially expand the fuel flexibility of gas turbines. The methane content in combusted fuel was varied from 0% to 30% in steps of 10% with a corresponding variation in the biodiesel fraction. In all cases, both fuels were combined, based on energy share ratio, to deliver a global heat output of 15 kW. Chemiluminescence imaging of C_2* and CH* species in the flames show a variation in combustion zone properties as fuel compositions change. It would seem that among the biodiesel-methane dual fuel flames, the reaction zone area and length reduces as methane fraction increases suggesting an overall reduction in reactivity and flame residence time in the combustion zone. Chemical kinetics analysis support this by predicting decreasing volumetric heat release rate and diminishing adiabatic flame temperature as gas fraction in fuel mix increases. The temporal variation of radical chemiluminescence integral intensity suggest that multiphase fuel burn in swirl-stabilised gas turbine combustors promotes flame stability and potentially lessens combustion noise as the fluctuation in the C_2* and CH* species integral intensity diminishes with higher methane content in the combustion process. Moreover, NO_x emissions were found to reduce in the dual fuel cases compared to neat biodiesel combustion and among the dual fuel cases, the NO_x emissions tend to decrease with increase in methane content of combusted fuel. Unburned hydrocarbon emissions, however, follow the opposite trend suggesting a depreciation of combustion efficiency with biodiesel/methane dual phase fuel burn compared to just the neat liquid fuel combustion. Furthermore, flame stability limits were found to contract as methane was introduced into the swirling air flow. Also, direct flame luminosity images suggest that multiphase fuel burn in swirl-stabilised gas turbine combustors result in wrinkling and flame brush separation.

Acknowledgement

Mr. Malcolm Seaborne, Mr. Paul Malpas and Ms. Amie Parnell are thankfully acknowledged for their help in construction and installation of the dual fuel burner. We appreciate the help of Mr Jose Ladera in capturing the actual flame images. Ogbonnaya Agwu is grateful to the Petroleum Technology Development Fund (PTDF) for sponsoring his PhD studies at Cardiff University.

References

[1] Chauhan BS, Kumar N, Cho HK. A study on the performance and emission of a diesel engine fueled with Jatropha biodiesel oil and its blends. *Energy* 37 (2012) 616-622.

[2] Hashimoto N, Ozawa Y, Mori N, Yuri I, Hisamatsu T. Fundamental combustion characteristics of palm methyl ester (PME) as alternative fuel for gas turbines. *Fuel* 87 (2008) 3373-3378.

[3] Rajasekar E, Murugesan A, Subramanian R, Nedunchezhian N. Review of NO(x) reduction technologies in CI engines fuelled with oxygenated biomass fuels. *Renew Sust Energy Rev* 14 (2010) 2113–2121.

[4] Agarwal AK. Biofuels (alcohols and biodiesel) applications as fuels for internal combustion engines. *Prog Energy Combust* 33 (2007) 233–271.

[5] He C, Ge YS, Tan JW, You KW, Han XK, Wang JF. Characteristics of polycyclic aromatic hydrocarbons emissions of diesel engine fueled with biodiesel and diesel. *Fuel* 89 (2010) 2040–2046.

[6] Di Y, Cheung CS, Huang ZH. Experimental investigation on regulated and unregulated emissions of a diesel engine fueled with ultra-low sulfur diesel fuel blended with biodiesel from waste cooking oil. *Sci Total Environ* 407 (2009) 835–846.

[7] Buyukkaya E. Effects of biodiesel on a DI diesel engine performance, emission and combustion characteristics. *Fuel* 89 (2010) 3099–3105.

[8] Ng JH, Ng HK, Gan SY. Characterisation of engine-out responses from a light duty diesel engine fuelled with palm methyl ester (PME). *Appl Energy* 90 (2012) 58–67.

[9] Sequera D, Agrawal AK, Spear SK, Daly DT. Combustion performance of liquid biofuels in a swirl-stabilized burner. *J. Eng. Gas Turbine. Power* 130 (2008) 032810-1-9.

[10] Erazo JA, Parthasarathy R, Gollahalli. Atomization and combustion of canola methyl ester biofuel spray. *Fuel* 89 (2010) 3735-3741.

[11] Chong CT, Hochgreb S. Flame structure, spectroscopy and emissions quantification of rapeseed biodiesel under model gas turbine conditions. *Appl Energy* 185 (2017) 1383-1392.

[12] An H, Yang WM, Chou SK, Chua KJ. Combustion and emissions characteristics of diesel engine fuelled by biodiesel at partial load conditions. *Appl Energy* 99 (2012) 363-371.

[13] Varatharajan K, Cheralathan M. Influence of fuel properties and composition on NOx emissions from biodiesel powered diesel engines: A review. *Renew Sust Energy Rev* 16 (2012) 3702-3710.

[14] The Royal Society. Sustainable biofuels: prospects and challenges. The Royal Society, London (2008).

[15] Department for Transport. Renewable Transport Fuel Obligation Annual Report 2014−15. The Stationery Office, London (2016).

[16] Archer SA, Murphy RJ, Steinberger-Wilckens R. Methodological analysis of palm oil biodiesel life cycle studies. *Renew Sust Energy Rev* 94 (2018) 694-704.

[17] Cheenkachorn K, Poompipatpong C, Ho CG. Performance and emissions of a heavy-duty diesel engine fuelled with diesel and LNG (liquid natural gas). *Energy* 53 (2013) 52-57.

[18] Srna A, Bolla M, Wright YM, Herrmann K, Bombach R, Pandurangi SS, Boulouchos K, Bruneaux G. Effect of methane on pilot-fuel auto-ignition in dual fuel engines. *Proc. Combust. Inst.* 37 (2019) 4741-4749.

[19] Papagiannakis RG, Hountalas DT. Experimental investigation concerning the effect of natural gas percentage on performance and emissions of a DI dual fuel diesel engine, *Appl. Therm. Eng*. 23 (2003) 353-365.

[20] Papagiannakis RG, Rakopoulos CD, Hountalas DT, Rakopoulos DC. Emission characteristics of high speed, dual fuel, compression ignition engine operating in a wide range of natural gas/diesel fuel proportions, *Fuel* 89 (2010) 1397-1406.

[21] Abedin MJ, Imran A, Masjuki HH, Kalam MA, Shahir SA, Varman M, Ruhul AM. An overview on comparative engine performance and emission characteristics of different techniques involved in diesel engine as dual-fuel engine operation. *Renew Sust Energy Rev* 60 (2016) 306-316.

[22] Kurji H, Valera-Medina A, Runyon J, Giles A, Pugh D, Marsh R, Cerone N, Zimbardi F, Valerio V. Combustion characteristics of biodiesel saturated with pyrolysis oil for power generation in gas turbines. *Renew Energy* 99 (2016) 443-451.
[23] Buffi M, Valera-Medina A, Marsh R, Pugh D, Giles A, Runyon J, Chiaramonti D. Emissions characterization tests for hydrotreated renewable jet fuel from used cooking oil and its blends. *Appl Energy* 201 (2017) 84-93.
[24] Habib Z, Pathasarathy R, Gollahalli S. Performance and emission characteristics of biofuel in a small-scale gas turbine engine. *Appl Energy* 87 (2010) 1701-1709.
[25] Rehman A, Phalke DR, Pandey R. Alternative fuel for gas turbine: Esterified jatropha oilediesel blend. *Renew Energy* 36 (2011) 2635-2640.
[26] Sidey J, Mastorakos E. Visualisation of turbulent swirling dual-fuel flames. *Proc. Combust. Inst*. 36 (2017) 1721-1727.
[27] Sidey JAM, Mastorakos E. Stabilisation of swirling dual-fuel flames. *Exp. Therm. Fluid Sci*. 95 (2018) 65-72.
[28] Evans MJ, Sidey JAM, Ye J, Medwell PR, Dally BB, Mastorakos E. Temperature and reaction zone imaging in turbulent swirling dual-fuel flames. *Proc. Combust. Inst.* 37 (2019) 2159-2166.
[29] Atabani AE, Silitonga AS, Badruddin IA, Mahlia TMI, Masjuki HH, Mekhilef S. A comprehensive review on biodiesel as an alternative energy resource and its characteristics. *Renew. Sustain. Energy Rev* 16 (2012) 2070-2093.
[30] Kumar N, Varun, Chauhan SR. Performance and emission characteristics of biodiesel from different origins: A review. *Renew. Sustain. Energy Rev* 21 (2013) 633-658.
[31] Alsulami R, Windell B, Nates S, Wang W, Won AH, Windom B. Investigating the role of atomization on flame stability of liquid fuels in an annular spray burner. *Fuel* 265 (2020) 116945.
[32] Kathrotia T, Riedel U, Siepel A, Moshammer K, Brockhinke A. Experimental and numerical study of chemiluminescent species in low-pressure flames, *Appl Phys B* 107 (2012) 571-584.
[33] Garcia-Armingol T, Hardalupas Y, Taylor AMKP, Ballester J. Effect of local flame properties on chemiluminescence-based stoichiometry measurement. *Exp. Therm. Fluid Sci* 53 (2014) 93-103.
[34] Morell MR, Seitzman J, Wilensky M, Lubarsky E, Lee J, Zinn B. Interpretation of optical emissions for sensors in liquid fuelled combustors. 39th Aerospace Sciences Meeting and Exhibit, Reno, NV, USA. AIAA-2001-0787.
[35] Ballester J, Garcia-Armingol T. Diagnostic techniques for the monitoring and control of practical flames. *Prog. Energy Combust. Sci* 36 (2010) 375-411.
[36] Runyon J, Marsh R, Bowen P, Pugh D, Giles A, Morris S. Lean methane flame stability in a premixed generic swirl burner: Isothermal flow and atmospheric combustion characterization. *Exp. Therm. Fluid Sci.* 92 (2018) 125-140.
[37] Reaction Design, CHEMKIN-PRO 15092. San Diego, California, 2009.
[38] Ranzi E, Frassoldati A, Stagni A, Pelucchi M, Cuoci A, Faravelli T. Reduced kinetic schemes of complex reaction systems: Fossil and biomass-derived transportation fuels. *International Journal of Chemical Kinetics* 46 (9) (2014) 512-542 DOI: 10.1002/kin.20867.
[39] Bergthorson JM, Thomson MJ. A review of the combustion and emissions properties of advanced transportation biofuels and their impact on existing and future engines. *Renew. Sustain. Energy Rev* 21 (2015) 1393-1417.
[40] Dryer FL. Chemical kinetic and combustion characteristics of transportation fuels. *Proc. Combust. Inst.* 35 (2017) 117-144.
[41] Fu X, Aggarwal SK. Fuel unsaturation effects on NOx and PAH formation in spray flames. *Fuel* 160 (2015) 1-15.
[42] Lefebvre AH, Ballal DR. Gas Turbine Combustion Alternative Fuels and Emissions, 3rd ed., CRC Press Taylor & Francis Group, 2010, p. 168.
[43] Syred N. A review of oscillation mechanisms and the role of the precessing vortex core (PVC) in swirl combustion systems. *Prog. Energy Combust. Sci* 32 (2006) 93-161.
[44] Valera-Medina A, Syred N, Bowen P. Central recirculation zone visualization in confined swirl combustors for terrestrial energy. *J Propul Power* 29 (1) (2013) DOI: 10.2514/1.B34600.
[45] Ballester J, Hernandez R, Sanz A, Smolarz A, Barroso J, Pina A. Chemiluminescence monitoring in premixed flames of natural gas and its blends with hydrogen. *Proc. Combust. Inst.* 32 (2009) 2983-2991.
[46] Razak AMY. Industrial gas turbines performance and operability. Woodhead publishing limited and CRC Press, 2007, p. 157.